GDCh Research Article Angewandte International Edition Chemie www.angewandte.org

How to cite: *Angew. Chem. Int. Ed.* **2024**, *63*, e202411224
doi.org/10.1002/anie.202411224

Batteries Hot Paper

A Highly Stable and Non-Flammable Deep Eutectic Electrolyte for High-Performance Lithium Metal Batteries

Li Zhao, Ao Xu, Yu Cheng, Hantao Xu, Lin Xu, and Liqiang Mai**

Abstract: Deep eutectic electrolytes (DEEs) are regarded as one of the next-generation electrolytes to promote the development of lithium metal batteries (LMBs) due to their unparalleled advantages compared to both liquid electrolytes and solid electrolytes. However, its application in LMBs is limited by electrode interface compatibility. Here, we introduce a novel solid dimethylmalononitrile (DMMN)-based DEE induced by N coordination to dissociate LiTFSI. We confirmed that the DMMN molecule can promote the dissociation of LiTFSI by the interaction between the N atom and Li^+, and form the hydrogen bond with $TFSI^-$ anion, which can promote the dissociation of LiTFSI to form DEE. More importantly, due to the absence of active α-hydrogen, DMMN exhibits greatly enhanced reduction stability with Li metal, resulting in favorable electrode/electrolyte interface compatibility. Polymer electrolytes based on this DEE exhibit high ionic conductivity (0.67 mS cm^{-1} at 25 °C), high oxidation voltage (5.0 V vs. Li^+/Li), favorable interfacial stability, and nonflammability. Li||LFP and Li||NCM811 full batteries utilizing this DEE polymer electrolyte exhibit excellent long-term cycling stability and excellent rate performance at high rates. Therefore, the new DMMN-based DEE overcomes the limitations of traditional electrolytes in electrode interface compatibility and opens new possibilities for improving the performance of LMBs.

[*] L. Zhao, A. Xu, Y. Cheng, H. Xu, Prof. L. Xu, Prof. L. Mai
State Key Laboratory of Advanced Technology for Materials Synthesis and Processing, School of Materials Science and Engineering,
Wuhan University of Technology,
Wuhan 430070, P.R. China
E-mail: linxu@whut.edu.cn
mlq518@whut.edu.cn
Prof. L. Xu, Prof. L. Mai
Hubei Longzhong Laboratory,
Wuhan University of Technology (Xiangyang Demonstration Zone),
Xiangyang 441000, Hubei, P.R. China
Prof. L. Xu, Prof. L. Mai
Hainan Institute,
Wuhan University of Technology,
Sanya 572000, P.R. China

Introduction

Lithium-ion batteries are extensively utilized in mobile phones, automobiles, and energy storage fields, promoting the development of the new energy industry.[1] However, due to the limited capacity of graphite anodes, the energy density of lithium-ion batteries cannot meet the needs of energy innovation.[2] Therefore, lithium metal batteries (LMBs) are regarded as the most likely candidate to meet the needs of energy innovation due to the high specific capacity of Li metal (3860 mAh g^{-1}) and low anode potential (−3.04 V vs. standard hydrogen electrode).[3] However, the commercial liquid electrolyte is flammable, which reduces the safety of LMBs.[4] Additionally, the organic solvent in the electrolyte easily reacts with Li metal, leading to problems such as poor interfacial compatibility.[5] Although solid electrolytes can avoid the use of solvents to improve battery safety, the interface problem with Li metal is still difficult to solve.[6] Therefore, there is a need to develop a new electrolyte system that is non-flammable, has high interfacial stability, high ionic conductivity, and a wide electrochemical window for application in LMBs.

Deep eutectic solvents (DESs) are mixtures of solid hydrogen bond acceptors and solid hydrogen bond donors in a certain molar ratio.[7] The robust intermolecular interactions within DESs, including hydrogen bonding, Lewis acid-base interactions, and van der Waals forces, result in a melting point (T_m) lower than that of individual components.[8] Metal-salt-incorporated deep eutectic electrolyte (DEE) systems are a distinct subset within the overarching domain of DESs.[9] As analogs of ionic liquids, DEEs have attracted much attention due to their non-flammability, good interfacial stability, high ionic conductivity, and wide electrochemical window.[10] Some DEEs based on Li salts (such as LiTFSI, $LiNO_3$, and $LiPF_6$) and hydrogen bond donors have been developed for LMBs.[11] DEEs currently reported mainly include the following types. Firstly, the formation of DEEs involves small molecules containing oxygen groups and lithium salts.[12] However, since the oxygen of $TFSI^-$ forms a clamp-shaped coordination structure with Li^+, it is difficult for the oxygen in other molecules to effectively dissociate LiTFSI through Li–O coordination, making it difficult to effectively improve battery performance. Secondly, urea or amide DEEs have attracted the attention of some researchers, in which the amino group and $TFSI^-$ anion form DEEs through hydrogen bonding.[13] However, amino groups easily react with Li metal, resulting in poor interfacial compatibility and difficulty in application. Thirdly, researchers focused their

attention on Li–N type DEEs, because the N atom has a lone pair of electrons and has a strong coordination ability with Li^+.[9–10] Nitrile (–C≡N) groups have attracted much attention as groups containing N atoms.[14] Succinonitrile (SN) molecules containing –C≡N groups are currently one of the most studied materials in DEEs.[15] SN has strong oxidation resistance because it contains –C≡N groups, but this also contains the active α-hydrogen in the SN molecule, increasing the reactivity with Li metal, resulting in the production of by-products that are detrimental to the stability of the electrode interface.[8b,11a,16] To improve the interfacial stability of DEEs containing –C≡N groups and prevent reaction with Li metal anode, current methods include combining SN with 1,3,5-trioxane and lithium difluoro (oxalato) borate (LiDFOB) to form a unique solvation structure to inhibit the reaction between SN and Li metal;[17] and SN and polyethylene glycol methyl ether acrylate (PEGMEA) to form DEE, using the interaction between the two to promote the dissociation of LiDFOB. The dissociation of LiDFOB can protect the Li metal interface and improve the interface stability of Li metal.[18] Another method is to use in situ polymerization to form chemically cross-linked polymers, dividing the SN-LiTFSI phase into nanoscale domains and confining them in the polymer to inhibit the interface reaction between SN and Li metal.[19] However, these methods are still difficult to completely avoid the reaction between the active α-hydrogen of SN molecules and Li metal.

In this study, we propose a novel solid dimethylmalononitrile (DMMN)-based DEE utilizing N coordination to induce dissociation of LiTFSI for use as an electrolyte for high-performance LMBs. Since the carbon atoms adjacent to –C≡N in the DMMN molecule do not contain H atoms, there is no active α-hydrogen, but there is β-hydrogen on a distant carbon atom. These β-hydrogen atoms are less affected by the electron-withdrawing effect of –C≡N, so they have better reduction stability with Li metal. Therefore, DMMN-based DEE exhibits greatly improved electrode compatibility. At the same time, DMMN is a new type of compound containing –C≡N groups. Its N atom possesses an unshared pair of electrons, which makes it have obvious advantages as an electron donor. Therefore, DMMN shows strong coordination with Li^+ and can promote the dissociation of LiTFSI. Moreover, the H atom in DMMN and the F atom in $TFSI^-$ anion can form hydrogen bonding interactions, which jointly induce the formation of DEE. In addition, adding a small amount of fluoroethylene carbonate (FEC), a reducible additive, builds a stable solid electrolyte interphase (SEI), which helps promote the stable cycling performance of DMMN-based DEE LMBs. The poly(vinylidene fluoride-co-hexafluoropropylene) (PVDF-HFP), polyethylene oxide (PEO), and LiTFSI were dissolved and dried to form a composite polymer electrolyte (PHPCPE). The DMMN-based DEE was then added to the PHPCPE and transformed into PHPCPE-DEE through thermal treatment (abbreviated as PHPDEE). The newly developed PHPDEE demonstrates an ionic conductivity of 0.67 $mS\,cm^{-1}$ at ambient conditions, exhibiting non-flammability and favorable interfacial stability. Li||$LiFePO_4$ (LFP) and Li||$LiNi_{0.8}Co_{0.1}Mn_{0.1}O_2$ (NCM811) batteries based on new DMMN-based DEE polymer electrolytes achieve superior rate performance and cycle stability, especially at high voltages. These results indicate that high-performance LMBs can be obtained with the new DMMN-based DEE polymer electrolyte.

Results and Discussion

Formation of DMMN-Based DEEs

The synthesis procedure for DMMN-based DEEs is simple and rapid (Figure 1a; Figure S1). The DEEs are denoted as DEE-1:n, where 1:n signifies the molar ratio of LiTFSI to DMMN. The thermal properties of DMMN-based DEE were studied using differential scanning calorimetry (DSC) and thermogravimetric analysis (TGA). The T_m of DEE-1:2 disappears in the DSC diagram, indicating that it has a longer liquefaction range and a lower glass transition temperature (−60.7 °C) (Figure 1b). As the molar fraction of LiTFSI decreases, a clear endothermic peak in the temperature range of 11.8 °C to 18.5 °C is evident in the DEE-1:4 to DEE-1:10, which indicates excess DMMN in DEE. These thermal properties data were used to construct a phase diagram of DEE (Figure 1c). The phase diagram illustrates the formation of a DEE between DMMN and LiTFSI, featuring a eutectic temperature of −60.7 °C and a lithium salt molar fraction near 0.33. In addition, the thermal stability of DEE was also characterized using TGA (Figure 1d; Figure S2). The results show that DEE exhibits two characteristic decomposition stages. The decomposition temperature of the first stage is 99–227 °C, and the decomposition temperature of the second stage is 410–430 °C. The decomposition temperatures of DMMN and LiTFSI are 125 and 426 °C, respectively. With the reduction in the molar fraction of LiTFSI in DEE, a noticeable decrease in the decomposition temperature of the initial stage is observed, suggesting an interaction between DMMN and LiTFSI. Besides, the weight loss of all DEEs after heating at 100 °C was less than 6 %, indicating that DEEs have good thermal adaptability.

The interaction between DMMN and LiTFSI helps the dissociation of LiTFSI and forms hydrogen bonding with $TFSI^-$ anion to induce the formation of DEE. Fourier transform infrared (FTIR) and Raman spectroscopy were applied to investigate the formation mechanism of DEE (Figure 1e–f). In pure DMMN, the FTIR at 2251 cm^{-1} corresponds to the stretching vibration of –C≡N.[14,20] When LiTFSI is added, the infrared bands of DEE-1:1 and DEE-1:2 move from 2251 cm^{-1} to 2282 cm^{-1}, indicating that there is an interaction between –C≡N groups and Li^+. As the DMMN molar ratio increases to DEE-1:4, 1:6, 1:8, and 1:10, the free DMMN band at 2551 cm^{-1} appears in the FTIR spectrum, indicating that the excess DMMN does not form coordination with Li^+. The coordination between DMMN and Li^+ has reached saturation. The peak at 2251 cm^{-1} in the Raman spectrum corresponds to the stretching vibration of –C≡N in free DMMN solvent.[8b]

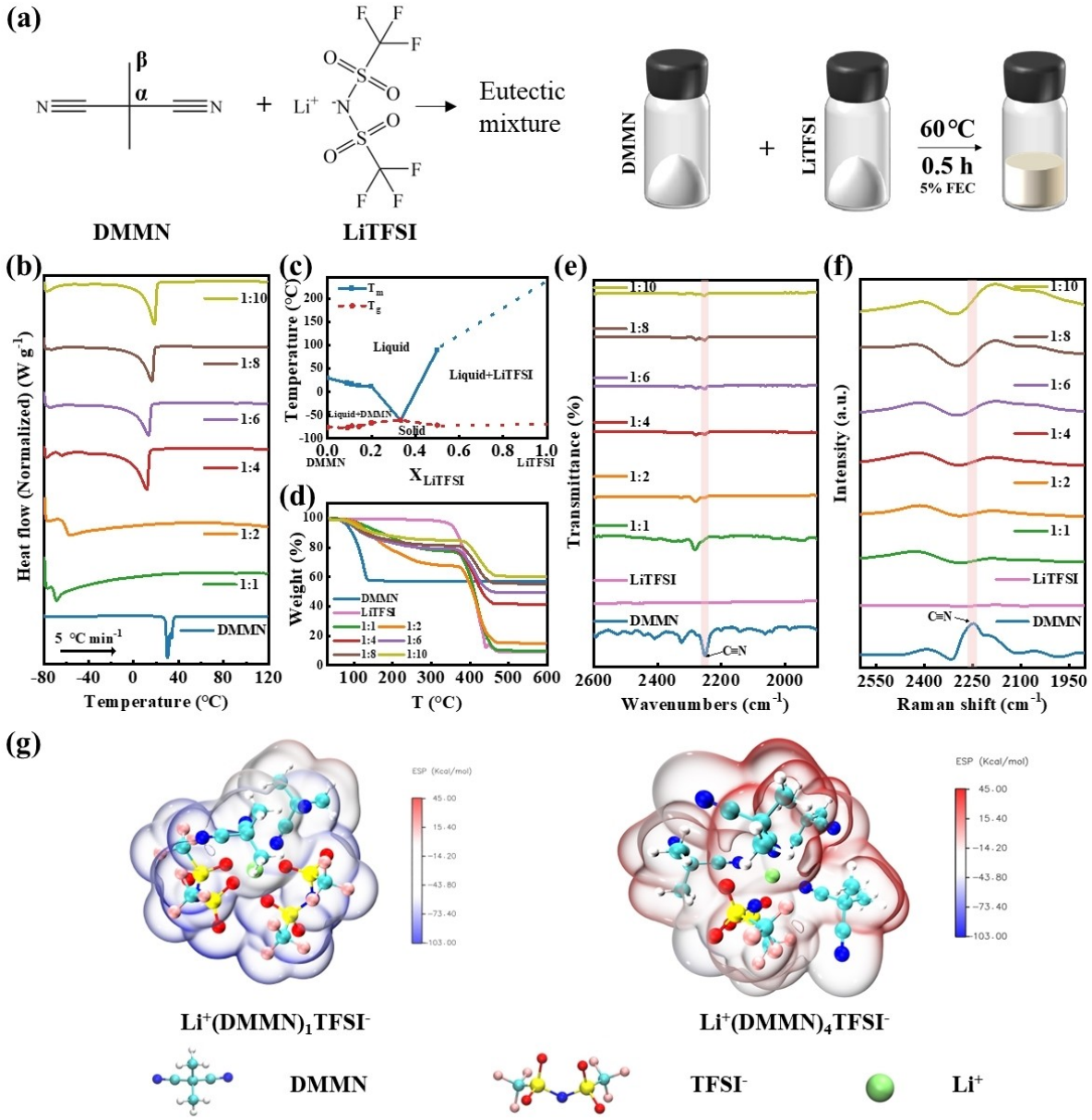

Figure 1. Formation of the LiTFSI/DMMN DEEs. a) Diagram of the preparation process of DEEs. b) DSC spectra of DEEs with a heating rate of 10 °C min^{-1} from −80 °C to 120 °C. c) Phase diagram of DEEs, DMMN, and LiTFSI. d) TGA spectra of DEEs from 30 °C to 600 °C with a heating rate of 10 °C min^{-1} under a nitrogen atmosphere. e)–f) FTIR and Raman spectra of DEEs. g) The molecular electrostatic potential energy surface of the Li(DMMN)$_n$TFSI complex. Atom colors: H-white, Li-green, C-cyan, N-blue, O-red, F-pink, S-yellow.

When the molar ratio of DMMN is DEE-1:1 and DEE-1:2, the –C≡N stretching vibration peak of free DMMN disappears. While from DEE-1:4 to DEE-1:10, the –C≡N stretching vibration peak reappears at 2183–2200 cm^{-1}. These results indicate that there is an interaction between –C≡N groups in DMMN molecules and Li^+.

In DEEs, as the molar fraction of DMMN increases, T_m first appears in DEE-1:4, and then T_m gradually increases. This shows that in DEE-1:4, DMMN is nearly coordinated with Li^+ in the lithium salt, and free DMMN just appears. Both FTIR and Raman spectroscopy results showed that excess DMMN started to appear in DEE-1:4. Based on the above results, DEE-1:4 is proposed to be the optimal DEE molar ratio.

Density functional theory (DFT) geometry optimization was conducted for $Li^+(DMMN)_1TFSI^-$ and $Li^+(DMMN)_4TFSI^-$ complexes to enhance comprehension of the coordination state of DMMN and Li^+ (Figure 1g). The results show that compared with $Li^+(DMMN)_1TFSI^-$, the $Li^+(DMMN)_4TFSI^-$ complex has lower molecular electrostatic potential energy and presents a more uniform surface distribution of molecular electrostatic potential energy. In $Li^+(DMMN)_4TFSI^-$, four N atoms in the DMMN molecule coordinate with Li^+. Compared with $Li^+(DMMN)_1TFSI^-$

complex in which Li^+ coordinates with two N atoms in DMMN and two O atoms in $TFSI^-$, the $Li^+(DMMN)_4TFSI^-$ complex exhibits an enhanced negative charge distribution among $TFSI^-$ anions. These results further confirm that the stability is optimal when Li^+ and DMMN form a 1:4 coordination state to generate DEE.

Revealing the Solvation Structure of DMMN-Based DEE

Nuclear magnetic resonance (NMR) spectroscopy was used to understand the local environmental changes of Li^+ to comprehensively elucidate the solvation structure of DMMN-based DEE (Figure 2a,b). After adding DMMN to LiTFSI, the ^7Li peak moves downfield from −0.87 ppm to −1.03 ppm, indicating that DMMN has an affinity for Li^+. In DEE-1:6, the ^7Li peak shifts upward to −1.027 ppm, indicating that the presence of too many free DMMN molecules in DEE changes the local environment of Li^+, which is not conducive to the coordination of Li^+. Furthermore, with the increase in the molar ratio of LiTFSI and DMMN in DEE, the ^{19}F peak gradually moves downfield from −78.71 ppm to −78.75 ppm. The moving distance suddenly becomes larger at DEE-1:4. This may be because from DEE-1:2 to DEE-1:4, the complete coordination between the N atom in DMMN and Li^+ promotes the dissociation of LiTFSI, weakens the coordination effect of $Li–F_{TFSI}^-$, and enhances the hydrogen bonding between the H atom in DMMN and the F atom in the free $TFSI^-$ anion. As the molar ratio of DMMN to LiTFSI continues to increase, the movement of the ^{19}F peak slows down significantly, which shows that increasing the molar fraction of DMMN after DEE-1:4 will weaken the coordination inhibition effect of $Li–F_{TFSI}^-$. Additionally, the characteristic peaks of FEC in the ^{19}F NMR spectrum remained unchanged at the positions corresponding to DEE-1:1 to DEE-1:10. The results show that FEC only plays a functional additive role in DEE (Figure S3). Radial distribution function (RDF) results of molecular dynamics (MD) simulations show (Figure S4a,b; Table S1) that $Li–F_{TFSI}^-$ in DEE-1:1 has a sharp peak at 2.22 Å, with a coordination number (CN) of 0.442. In DEE-1:4, the sharp peak of $Li–F_{TFSI}^-$ appears at 2.28 Å, and CN decreases to 0.096. These results indicate that the $Li–F_{TFSI}^-$ effect in DEE is weakened,

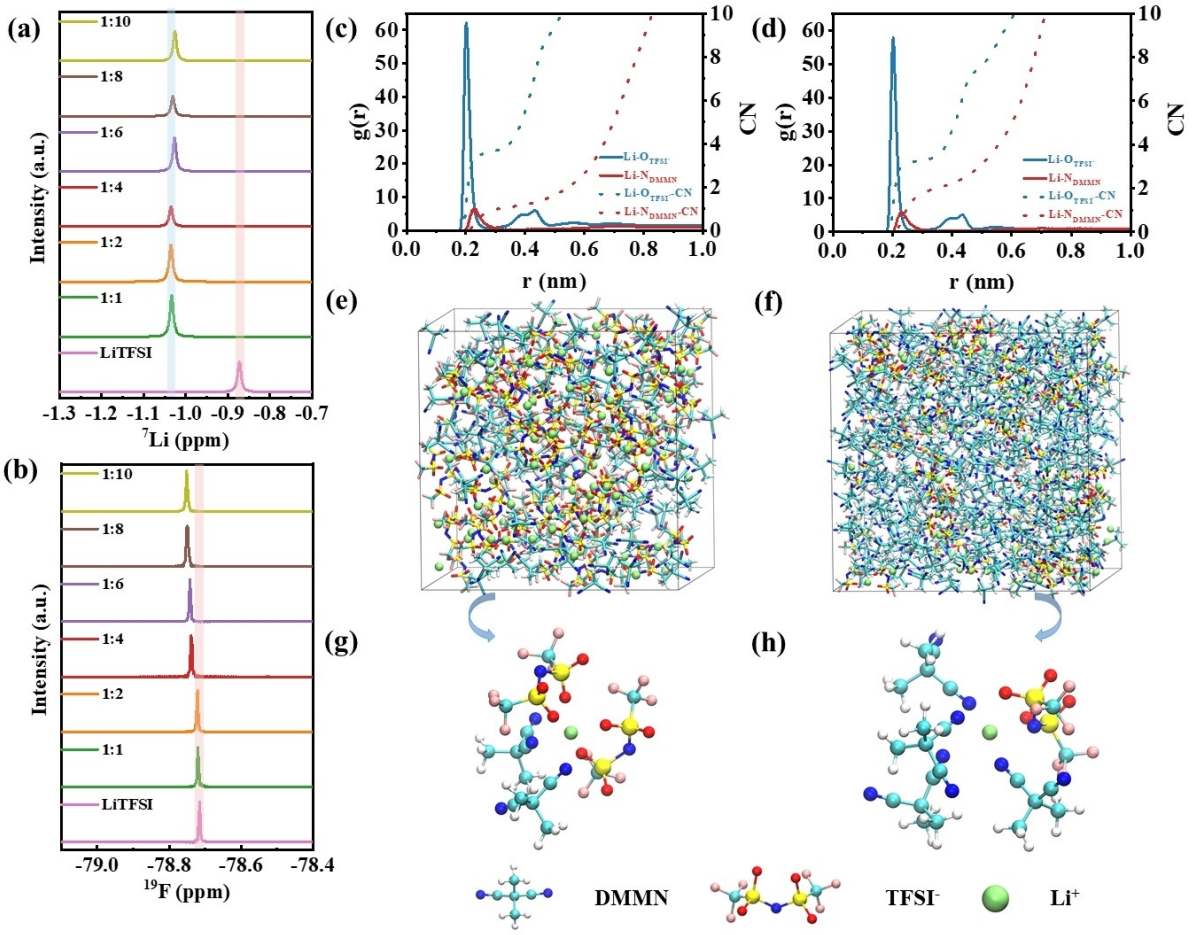

Figure 2. Revealing the solvation structure of the designed DEE. a)–b) NMR spectra of LiTFSI, LiTFSI in DMMN. c)–d) The radial distribution function of DEE-1:1 and DEE-1:4. e)–f) MD simulation snapshots of DEE-1:1 and DEE-1:4 obtained at 298 K. g)–h) Representative Li^+ complex structures (magnified local solvation structure during MD simulations) in DEE-1:1 and DEE-1:4. Atom colors: H-white, Li-green, C-cyan, N-blue, O-red, F-pink, S-yellow.

further proving that DEE-1:4 has better Li^+ coordination. In addition, the DMMN ^1H peak appears at 1.817 ppm (Figure S4c), while in DEE-1:1 to DEE-1:10, the ^1H peak moves upfield to 1.815 ppm, indicating that there is a hydrogen bonding interaction between H atoms in DMMN and F atoms in $TFSI^-$, which is also one of the reasons for the downward field movement of ^{19}F.

MD theory was used to calculate the two systems of DEE-1:1 and DEE-1:4 to further reveal the unique solvation structure of the DMMN-based DEE. The RDF results of MD simulations were first compared (Figure 2c, d). In DEE-1:1, Li-N_{DMMN} and Li-O_{TFSI}^- have sharp peaks at 2.26 Å and 2.02 Å, confirming that both DMMN and $TFSI^-$ can participate in Li^+ coordination. As the molar ratio of DEE increases to 1:4, the sharp peak of Li-N_{DMMN} in DEE increases to 2.60 Å. This shows that the increased radial distance between Li^+ and DMMN is beneficial to the desolvation process of Li^+ at the electrolyte/electrode interface and improves the Li^+ transference number of the DEE.[17] In addition, compared with the CN of Li-N_{DMMN} and Li-O_{TFSI}^- in DEE-1:1 which are 0.969 and 3.669, the CN of Li-N_{DMMN} in DEE-1:4 increases to 1.781 and the CN of Li-O_{TFSI}^- decreases to 3.268 (Table S2). This shows that DMMN molecules have coordination with Li^+ and can promote the dissociation of LiTFSI. DEE-1:1 and DEE-1:4 were then studied through MD simulations to explore the solvation structure of Li^+. The comprehensive MD simulation findings of the formulated DEE indicate that in DEE-1:1, the final optimized Li^+ first coordination shell is Li^+-DMMN-$TFSI^-$ (Figure 2e,g). Compared with DEE-1:1, the most stable solvation configuration in DEE-1:4 involves one Li^+ coordinated by one $TFSI^-$ anion and four DMMN molecules (Figure 2f,h). The competitive relationship between DMMN and $TFSI^-$ increases the transport of Li^+, giving DEE better ionic conductivity.

Characterizations of the PHPDEE Polymer Electrolytes

DEE was incorporated with polymers to generate DEE/polymer composite electrolyte. As a carrier of DEE, the polymer composite electrolyte has the advantages of high strength and good wettability, which can effectively prevent battery short circuits and improve battery cycle stability (Figure S5a,b). To keep the composite electrolyte with an optimized molar ratio of LiTFSI to DMMN in polymers, PHPDEE-1:4 polymer electrolyte was obtained by the reaction between DMMN in DEE-1:6 and LiTFSI (Figure S6). To characterize the performance of PHPDEE-1:4, EIS was used to test the ionic conductivity of PHPCPE, PHPCPE added with DEE-1:6 at 25 °C for 24 h, and PHPCPE added with DEE-1:6 at 60 °C for 0.5 h. It can be seen from the Nyquist plot that with the addition of DEE-1:6 to PHPCPE, the polymer electrolyte heated at 60 °C for 0.5 h has the highest ionic conductivity (Figure S7a). In addition, the temperature-dependent electrochemical impedance spectroscopy test of PHPDEE-1:4 showed that its ionic conductivity maintains good adaptability with temperature (Figure S7b). Besides, the interfacial activation energy of PHPDEE-1:4 (34.38 kJ mol^{-1}) is significantly lower than that of PHPCPE (52.47 kJ mol^{-1}) (Figure S7c). This shows that adding DEE-1:6 to PHPCPE and heating at 60 °C for 0.5 h can obtain PHPDEE-1:4 with stable performance.

The ionic conductivity of DEEs at different temperatures was measured using temperature-dependent EIS to further analyze the temperature adaptability of different molar ratios of PHPDEE (Figure 3a). With the increase in DMMN content in DEEs, the ionic conductivity gradually increases and maintains a good linear relationship with temperature. Among them, the ionic conductivity increases significantly slower from PHPDEE-1:6 to PHPDEE-1:10. In addition, the Nyquist curves of PHPDEE-1:4 at different temperatures also show good temperature adaptability (Figure 3b). At room temperature, with the increase of DMMN content in DEEs, the ionic conductivity of PHPDEEs rapidly increases from 2.37×10^{-5} S cm^{-1} of PHPDEE-1:1 to 6.74×10^{-4} S cm^{-1} of PHPDEE-1:4, and then the growth rate slowed down from PHPDEE-1:4 to PHPDEE-1:10, and the ionic conductivity of PHPDEE-1:10 is 7.08×10^{-4} S cm^{-1} (Figure S8a,b). This is because the molar ratio of LiTFSI to DMMN is lower than DEE-1:4, there is no free DMMN in the solution, and the dissociation degree of LiTFSI is low, so the ionic conductivity is low. When the molar ratio of LiTFSI to DMMN reaches 1:4, a small amount of free DMMN appears, which weakens the intermolecular interaction between the Li^+(DMMN) complex cation and $TFSI^-$ anion in DEE, effectively promoting the dissociation of lithium salts. However, continuing to increase the molar fraction of DMMN in DEEs will reduce the density of carriers (Li^+), so the increase in ionic conductivity slows down from DEE-1:4 to DEE-1:10.[9] Therefore, PHPDEE electrolyte has good temperature adaptability.

Electrochemical stability represents another pivotal aspect in assessing the appropriateness of an electrolyte. The electrochemical stability of PHPCPE and PHPDEE at ambient conditions was assessed via linear sweep voltammetry (LSV) (Figure 3c). Compared with PHPCPE, PHPDEE-1:4 has a higher oxidation voltage, reaching 5.0 V. This is because the triple bond structure of –C≡N gives it high electron affinity and stability, making it less prone to oxidation reactions. Additionally, the absence of α-hydrogen atoms in the DMMN molecule ensures excellent stability during reduction with Li metal, resulting in a highly compatible and stable interface between PHPDEE and the Li metal anode. Therefore, DMMN-based PHPDEE-1:4 has a wide electrochemical window. The exchange current density in PHPDEE-1:4 (0.41 mA cm^{-2}) obtained by fitting the Tafel curve is significantly higher than that of PHPCPE (0.29 mA cm^{-2}), suggesting enhanced charge transfer kinetics. Fast charge transfer is beneficial for better battery performance (Figure 3d). This may be because DEE-1:4 can effectively wet the interface and has good interface stability with Li metal. In addition, the Li^+ transference number of PHPDEE-1:4 is 0.31, which is higher than the value of PHPCPE of 0.24 (Figure S9; Table S3), which indicates that the competitive relationship between DMMN and $TFSI^-$ can increase the Li^+ transference number of PHPDEE.

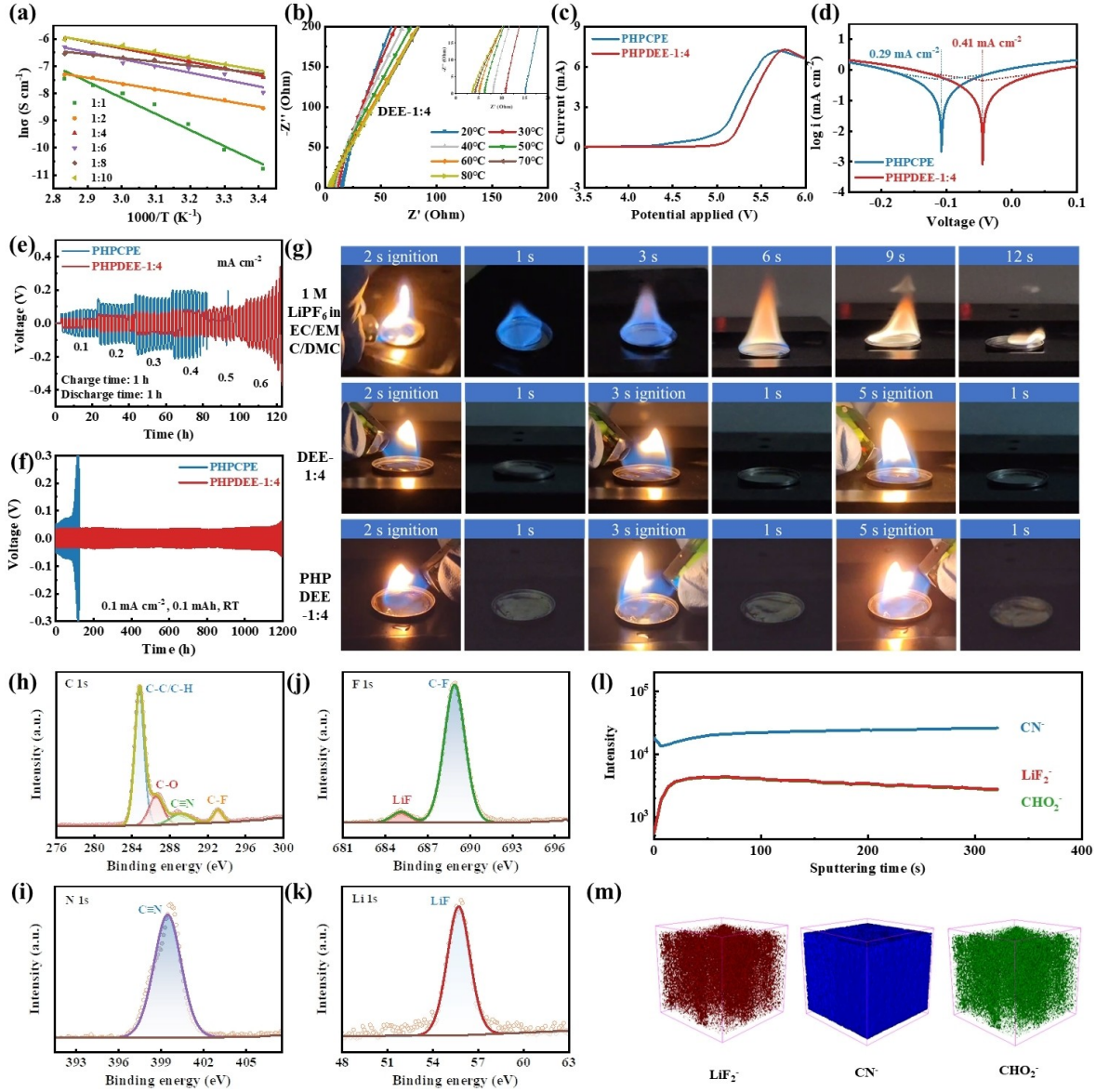

Figure 3. Characterizations of the PHPDEEs. a) Temperature-dependent ionic conductivity of the PHPDEEs. b) Nyquist plots of the PHPDEE-1 : 4 collected at different temperatures. c) LSVs of the PHPDEE-1 : 4 using stainless steels as the working electrode and Li as the counter/reference electrodes at a scan rate of 10 mV s^{-1}. d) Tafel plots obtained from CV test in Li||Li cell using the PHPDEE-1 : 4. e) Rate performance test of the Li||Li symmetric cells at various current densities from 0.1 to 0.6 mA cm^{-2}. f) Voltage profiles of the Li||Li symmetric cells using the PHPDEE-1 : 4 at 0.1 mA cm^{-2} for 1 h. g) Optical images of the ignition of commercial organic electrolyte (1 M $LiPF_6$ in EC/EMC/DMC (1/1/1 by weight)), the DEE-1 : 4, and PHPDEE-1 : 4. h)–k) C 1s (h), N 1s (i), F 1s (j), and Li 1s (k) XPS spectra of the Li||Li symmetric cells using PHPDEE-1 : 4 after cycles. l)-m) TOF-SIMS negative ion depth profiles and compiled a 3D diagram of cycled Li anode harvested from the cycled Li||Li symmetric cells using PHPDEE-1 : 4.

The mechanism of the better electrochemical performance of DMMN-based DEE was studied by analyzing the compatibility of DMMN-based DEE and Li metal anode. The interfacial compatibility of DMMN-based DEE is significantly influenced by the reduction stability of DMMN. To quantify this, the DFT was used to calculate the energy required to break the C–H bond in DMMN and SN (Figure S10a,b). The results show that the energy of breaking the C–H bond in DMMN is 16.5 eV, which is higher than the 15.5 eV in commonly used SN molecules. This shows that DMMN has better stability to Li metal than SN. This may be because the strongly electron-withdrawing –C≡N has an affinity for the negatively charged α-carbon, which significantly enhances the activity of the α-hydrogen. Therefore, the α-hydrogen atoms on α carbons adjacent to –C≡N may be more susceptible to detachment. The presence of α-hydrogen in the molecule will make the molecule highly reactive when in contact with the highly reducing Li metal, generating hydrogen gas and may produce undesirable interface by-products. Even more, the generated lithium nitrile with negatively charged α-carbon will further react with other nitriles to form conjugated

oligomers and polymers, causing the performance of LMB to decay rapidly. In contrast, DMMN does not contain α-hydrogen but contains β-hydrogen that is far away from –C≡N. Since β-hydrogen is less affected by –C≡N, DMMN molecules have higher reduction stability. Therefore, DMMN-based DEE has better electrochemical performance than SN-based DEE (Figure S11a–d; Table S4, 5). In addition, there was no obvious change after immersing the Li metal in DMMN-based DEE-1:4 for 90 days, indicating the excellent reduction stability of DMMN-based DEE (Figure S12, 13).

Li||Li symmetric cell with PHPDEE was assembled to further study the compatibility of DEE with Li metal anode. The interfacial stability was investigated by performing lithium galvanostatic plating/stripping cycles on Li||Li symmetric cells (Figure 3e). The voltage profile of galvanostatic plating/stripping with current density increasing from 0.1 mA cm^{-2} to 0.6 mA cm^{-2} was recorded. The polarization voltage curve increases with increasing current density, and even at 0.6 mA cm^{-2}, the cell still maintains stable cycling without short-circuiting. Compared with the rate performance of PHPCPE, it has obvious rate performance advantages. The Li||Li symmetric cell of PHPDEE-1:4 was further tested. At a current density of 0.1 mA cm^{-2}, the overpotential remained stable within 850 h, indicating that the SEI formed under PHPDEE-1:4 is relatively stable (Figure 3f). Furthermore, at a current density of 0.1 mA cm^{-2}, the Li||PHPDEE-1:4||Li cell exhibited stable Li plating/stripping over 1200 h and remained stable during cycling without short-circuiting. The above test results indicate that PHPDEE-1:4 has good interfacial compatibility and electrochemical stability. In addition, at current densities of 0.2, 0.3, and 0.5 mA cm^{-2}, Li||PHPDEE-1:4||Li cells have better cycle stability than PHPCPE (Figure S14), further indicating that PHPDEE has good interfacial compatibility and electrochemical stability.

The thermal safety of the electrolyte is critical to LMBs. The flammability of commercial liquid electrolytes, DEE-1:4 and PHPDEE-1:4 was tested (Figure 3g). Commercial liquid electrolytes can be ignited within 2 seconds, while DEE-1:4 and PHPDEE-1:4 cannot be ignited even if the ignition time is extended to 5 seconds, suggesting the intrinsic safety superiority of DEE-1:4 and PHPDEE-1:4 over commercial liquid electrolytes. As a result, a deep eutectic polymer electrolyte was successfully developed, which is safe and exhibits excellent interfacial stability.

In order to analyze the interfacial compatibility and electrochemical stability of PHPDEE and Li metal anode, X-ray photoelectron spectroscopy (XPS) was used to study the SEI composition after cycling (Figure 3h–k). The C 1s spectrum shows four peaks, representing C–F, C≡N, C–O, and C–C/C–H, respectively, revealing the presence of organic products in the SEI layer. In the F 1s spectrum, the main peak is located at 685 eV, corresponding to LiF. The N 1s spectrum shows that the main peak of C≡N is located at 399.5 eV,[8b,17] and no products of –C≡N decomposition were found, which shows that DMMN molecules and Li metal have good reduction stability. Li 1s XPS results also confirmed LiF in the SEI layer. LiF mainly comes from the reaction between FEC and the interface. As a robust inorganic compound, it contributes to augmenting the mechanical strength of the SEI layer. More importantly, LiF significantly enhances the ionic transport capacity of SEI, thereby greatly improving the stability of the interface between PHPDEE and Li metal anode.[21] These results are helpful in achieving highly reversible Li deposition/stripping in Li metal batteries using PHPDEE as an electrolyte.

The chemical composition and microstructure of the SEI layer were additionally verified utilizing time-of-flight secondary-ion mass spectrometry (TOF-SIMS). According to the depth profile and three-dimensional distribution map (Figure 3l,m), it is found that the inorganic component LiF_2^- is evenly distributed in the SEI, and the CN^- fragments fill the entire Li metal surface layer. In addition, the organic component CHO_2^- is also uniformly distributed on the Li metal surface. Since the FEC additive helps form a thin and strong SEI film,[22] the inorganic component LiF_2^- and the organic component CHO_2^- are mainly derived from the reaction of FEC with Li metal. Furthermore, the large amount of CN^- fragments in DMMN indicates that DMMN-based DEE still has good interfacial stability with Li metal under the condition of applied voltage. These identified rigid inorganic species, such as LiF, along with flexible organic components, collectively establish a robust and elastic SEI protective layer, thereby enhancing the stability and cyclability of the Li metal anode.

Battery Performances with the PHPDEE Polymer Electrolytes

Li||LFP batteries were assembled to evaluate the potential application value of PHPDEE in LMBs. The results show that the LFP battery using PHPDEE-1:4 exhibits good rate performance at room temperature (Figure 4a,b). Li||PHPDEE-1:4||LFP batteries exhibit highly reversible specific capacities of 167, 159, 151, 142, 135 and 127 mAh g^{-1} at 0.2, 0.5, 1.0, 2.0, 3.0 and 5.0 C, respectively. Upon returning the current density to 0.2 C, the specific capacity can be fully restored to 168 mAh g^{-1} without capacity loss. In comparison, the specific capacities of LFP batteries with PHPCPE electrolyte at the same rate were 130, 119, 86, 34, 14, and 4 mAh g^{-1}, respectively. This indicates that PHPDEE-1:4 has a better rate performance than PHPCPE. In addition, the cycling stability of Li||PHPDEE-1:4||LFP batteries was evaluated at rates of 0.5, 1.0, and 2.0 C (Figure 4c; Figure S15a,b). At a rate of 0.5 C, after 550 cycles, the Li||PHPDEE-1:4||LFP battery has a reversible capacity of 149 mAh g^{-1} and a capacity retention rate of 99.1 %. At a rate of 1.0 C, after 800 cycles, the reversible capacity of the Li||PHPDEE-1:4||LFP battery is 146 mAh g^{-1}, with no capacity fading. At a rate of 2.0 C, after 750 cycles, the reversible capacity of Li||PHPDEE-1:4||LFP battery is 125 mAh g^{-1}, with no capacity degradation. The batteries with PHPDEE exhibit superior performance compared to those with PHPCPE across all three rates. These results benefit from the good interfacial wettability and electrochemical stability of PHPDEE.

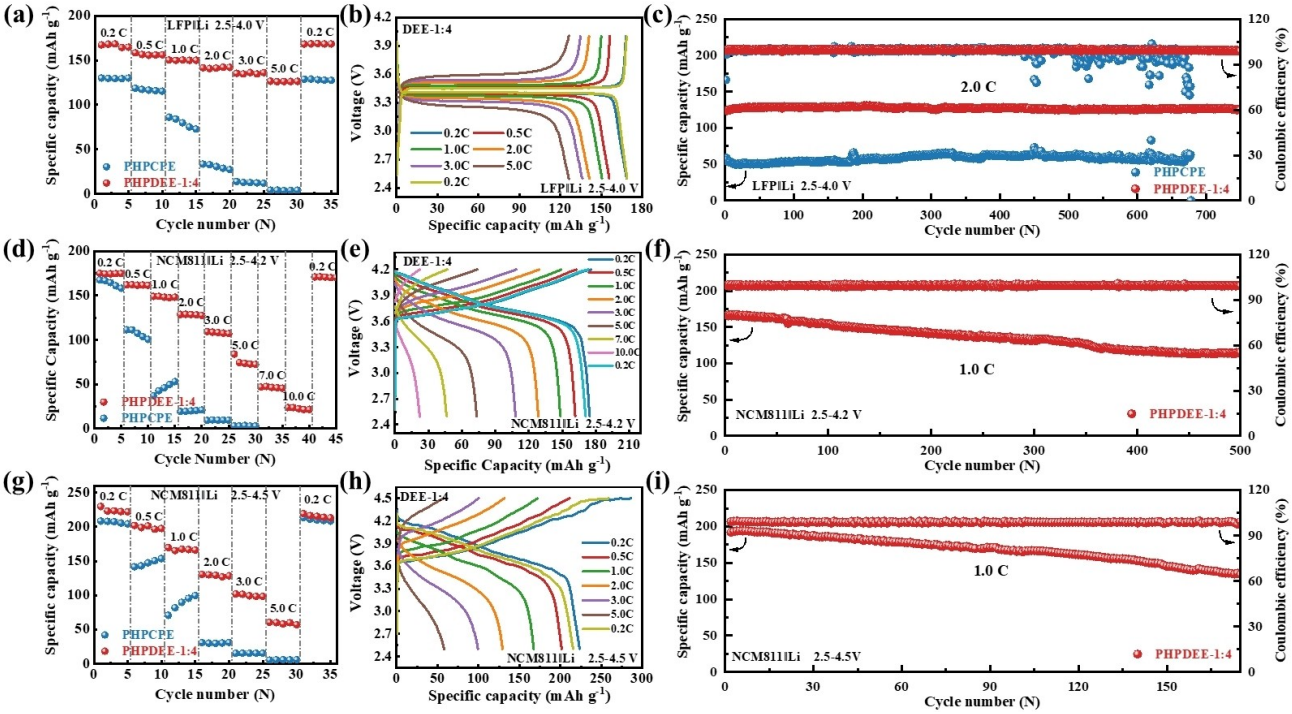

Figure 4. Battery performances of the PHPDEE in full batteries. a)–b) Rate performance and charge–discharge profiles of LFP||Li batteries. c) Long-term cycling performance of the LFP||Li batteries at 2 C under room temperature. d)–e) Rate performance and charge–discharge profiles of NCM811||Li batteries. f) Long-term cycling performance of the NCM811||Li batteries at 1 C under room temperature. g)–h) Rate performance and charge–discharge profiles of NCM811||Li batteries within the voltage range of 2.5–4.5 V. i) Long-term cycling performance of the NCM811||Li batteries at 1 C within the voltage range of 2.5–4.5 V under room temperature. PHPDEE with an optimized molar ratio of LiTFSI to DMMN (1 : 4) was applied in these batteries.

The rate performance of NCM 811 batteries using PHPDEE was tested at room temperature to further verify the broad application of PHPDEE (Figure 4d,e). The results show that Li||PHPDEE-1 : 4||NCM811 battery exhibits highly reversible specific capacities at 0.2, 0.5, 1.0, 2.0, 3.0, 5.0 and 10.0 C, which are 175, 162, 149, 129, 109, 74, 47 and 24 mAh g^{-1}, respectively. When the current density returns to 0.2 C, the specific capacity can be restored to 171 mAh g^{-1}, with extremely high-capacity retention. Furthermore, even when utilizing a high-loading NCM811 cathode, the Li||PHPDEE-1 : 4||NCM811 battery still exhibits good rate performance (Figure S16). In addition, the cycling stability of NCM811 batteries using PHPDEE-1 : 4 was evaluated at 0.5, 1.0, and 2.0 C (Figure 4f; Figure S17a,b). At a rate of 1.0 C, the Li||PHPDEE-1 : 4||NCM811 battery has a reversible capacity of 116 mAh g^{-1} after 500 cycles, and the capacity retention rate is 70 %. It also has a capacity retention rate of 70 % when cycled 450 times at a rate of 0.5 C and 170 times at a rate of 2.0 C. When the charge and discharge range of the NCM811 battery was increased to 2.5–4.5 V, the NCM811 battery using PHPDEE-1 : 4 still showed good rate and cycle performance (Figure 4g–i; Figure S18a,b). Moreover, the cycling performance of full batteries with PHPDEE-1 : 4 is superior to that of full batteries with PHPCPE containing liquid electrolytes (Figure S19). This shows that PHPDEE has good electrochemical stability. Comprehensive performance test results show that PHPDEE exhibits good performance in full batteries and has broad application prospects in both LFP and NCM811 materials.

Conclusion

In summary, a solid DMMN-based DEE with N coordination-induced dissociation of LiTFSI was successfully developed as an electrolyte for high-performance LMBs. Experimental results show that DMMN exhibits robust coordination with Li^+ and forms hydrogen bonding interactions with $TFSI^-$ anions, inducing the dissociation of lithium salts to form DEE. MD simulation results show that the –C≡N group in DMMN is more inclined to coordinate with Li^+ to form a Li^+-DMMN complex. Since DMMN contains relatively stable β-hydrogen, DMMN-based DEE has better reduction stability with Li metal. At a molar ratio of LiTFSI and DMMN of 1 : 4, the PHPDEE polymer electrolyte demonstrates outstanding characteristics, including high ionic conductivity (0.67 mS cm^{-1} at 25 °C), stable interfacial properties, and non-flammability. The LFP battery assembled using PHPDEE polymer electrolyte can stably cycle 750 times at a rate of 2.0 C with almost no degradation, while the NCM811 battery can reach a maximum rate of 10.0 C, showing excellent rate performance. Even when the voltage rises to 4.5 V, the NCM811

battery still has a good rate and cycle performance, showing that PHPDEE has a wide voltage range. This research provides a promising new solution for deep eutectic polymer electrolytes and provides strong support for the practical application of high-performance LMBs.

Acknowledgements

This work was supported by the National Natural Science Foundation of China (52272234), the National Key Research and Development Program of China (2020YFA0715000), the Key Research and Development Program of Hubei Province (2021BAA070), independent Innovation Projects of the Hubei Longzhong Laboratory (2022ZZ-20) and the Sanya Science and Education Innovation Park of Wuhan University of Technology (2021KF0011).

Conflict of Interest

The authors declare no conflict of interest.

Data Availability Statement

The data that support the findings of this study are available from the corresponding author upon reasonable request.

Keywords: dimethylmalononitrile · nitrile group · deep eutectic electrolytes · stable interfacial compatibility · lithium metal batteries

[1] a) T. Zhu, H. Sternlicht, Y. Ha, C. Fang, D. Liu, B. H. Savitzky, X. Zhao, Y. Lu, Y. Fu, C. Ophus, C. Zhu, W. Yang, A. M. Minor, G. Liu, *Nat. Energy* **2023**, *8*, 129–137; b) B. L. D. Rinkel, J. P. Vivek, N. Garcia-Araez, C. P. Grey, *Energy Environ. Sci.* **2022**, *15*, 3416–3438; c) P. Shi, J. Ma, M. Liu, S. Guo, Y. Huang, S. Wang, L. Zhang, L. Chen, K. Yang, X. Liu, Y. Li, X. An, D. Zhang, X. Cheng, Q. Li, W. Lv, G. Zhong, Y.-B. He, F. Kang, *Nat. Nanotechnol.* **2023**, *18*, 602–610.

[2] a) H. Cheng, Z. Ma, P. Kumar, H. Liang, Z. Cao, H. Xie, L. Cavallo, Q. Li, J. Ming, *ACS Energy Lett.* **2024**, 1604–1616; b) H. Li, F. Zhang, W. Wei, X. Zhao, H. Dong, C. Yan, H. Jiang, Y. Sang, H. Chen, H. Liu, S. Wang, *Adv. Energy Mater.* **2023**, *13*, 2301023; c) W. Chen, R. V. Salvatierra, J. T. Li, C. Kittrell, J. L. Beckham, K. M. Wyss, N. La, P. E. Savas, C. Ge, P. A. Advincula, P. Scotland, L. Eddy, B. Deng, Z. Yuan, J. M. Tour, *Adv. Mater.* **2023**, *35*, e2207303.

[3] a) S. Chai, Y. Zhang, Y. Wang, Q. He, S. Zhou, A. Pan, *eScience* **2022**, *2*, 494–508; b) H. Wang, Y. Yang, C. Gao, T. Chen, J. Song, Y. Zuo, Q. Fang, T. Yang, W. Xiao, K. Zhang, X. Wang, D. Xia, *Nat. Commun.* **2024**, *15*, 2500; c) G. Wang, Y. Liang, H. Liu, C. Wang, D. Li, L. Z. Fan, *Interdiscip. Mater.* **2022**, *1*, 434–444.

[4] a) D. Wang, H. Xie, Q. Liu, K. Mu, Z. Song, W. Xu, L. Tian, C. Zhu, J. Xu, *Angew. Chem. Int. Ed.* **2023**, *62*, e202302767; b) X. Zhang, P. Xu, J. Duan, X. Lin, J. Sun, W. Shi, H. Xu, W. Dou, Q. Zheng, R. Yuan, J. Wang, Y. Zhang, S. Yu, Z. Chen, M. Zheng, J.-F. Gohy, Q. Dong, A. Vlad, *Nat. Commun.* **2024**, *15*, 536; c) G.-R. Zhu, Q. Zhang, Q.-S. Liu, Q.-Y. Bai, Y.-Z. Quan, Y. Gao, G. Wu, Y.-Z. Wang, *Nat. Commun.* **2023**, *14*, 4617.

[5] a) X. Hu, Y. Ma, J. Qian, W. Qu, Y. Li, R. Luo, H. Wang, A. Zhou, Y. Chen, K. Shi, L. Li, F. Wu, R. Chen, *Adv. Mater.* **2023**, *36*, e2303710; b) Y. Huang, R. Li, S. Weng, H. Zhang, C. Zhu, D. Lu, C. Sun, X. Huang, T. Deng, L. Fan, L. Chen, X. Wang, X. Fan, *Energy Environ. Sci.* **2022**, *15*, 4349–4361; c) X. Zhou, F. Huang, X. Zhang, B. Zhang, Y. Cui, Z. Wang, Q. Yang, Z. Ma, J. Liu, *Angew. Chem. Int. Ed.* **2024**, *63*, e202401576.

[6] a) F. Ren, Z. Liang, W. Zhao, W. Zuo, M. Lin, Y. Wu, X. Yang, Z. Gong, Y. Yang, *Energy Environ. Sci.* **2023**, *16*, 2579–2590; b) L. Zhang, Y. Liu, Y. You, A. Vinu, L. Mai, *Interdiscip. Mater.* **2022**, *2*, 91–110; c) Q. Luo, L. Ming, D. Zhang, C. Wei, Z. Wu, Z. Jiang, C. Liu, S. Liu, K. Cao, L. Zhang, C. Yu, S. Cheng, *Energy Mater. Adv.* **2023**, *4*, 0065.

[7] a) L. Chao-Le, G. Huang, Y. Yu, Q. Xiong, J.-M. Yan, X.-B. Zhang, *J. Am. Chem. Soc.* **2022**, *144*, 5827–5833; b) A. L. Phan, C. Jayawardana, P. M. L. Le, J. Zhang, B. Nan, W. Zhang, B. L. Lucht, S. Hou, C. Wang, *Adv. Funct. Mater.* **2023**, *33*, 2301177.

[8] a) H. Guo, L. Li, X. Xu, M. Zeng, S. Chai, L. Wu, H. Li, *Angew. Chem. Int. Ed.* **2022**, *61*, e202210695; b) Q. Hou, P. Li, Y. Qi, Y. Wang, M. Huang, C. Shen, H. Xiang, N. Li, K. Xie, *ACS Energy Lett.* **2023**, *8*, 3649–3657.

[9] X. Pei, Y. Li, T. Ou, X. Liang, Y. Yang, E. Jia, Y. Tan, S. Guo, *Angew. Chem. Int. Ed.* **2022**, *61*, e202205075.

[10] J. Song, Y. Si, W. Guo, D. Wang, Y. Fu, *Angew. Chem. Int. Ed.* **2021**, *60*, 9881–9885.

[11] a) P. Prakash, B. Fall, J. Aguirre, L. A. Sonnenberg, P. R. Chinnam, S. Chereddy, D. A. Dikin, A. Venkatnathan, S. L. Wunder, M. J. Zdilla, *Nat. Mater.* **2023**, *22*, 627–635; b) H. Moon, S. J. Cho, D. E. Yu, S. Y. Lee, *Energy Environ. Mater.* **2022**, *6*, e12383.

[12] a) P. Dong, X. Zhang, K. S. Han, Y. Cha, M.-K. Song, *J. Energy Chem.* **2022**, *70*, 363–372; b) M. Li, H. An, Y. Song, Q. Liu, J. Wang, H. Huo, S. Lou, J. Wang, *J. Am. Chem. Soc.* **2023**, *145*, 25632–25642; c) Y. Wang, R. Xu, B. Xiao, D. Lv, Y. Peng, Y. Zheng, Y. Shen, J. Chai, X. Lei, S. Luo, X. Wang, X. Liang, J. Feng, Z. Liu, *Mater. Today Phys.* **2022**, *22*, 100620.

[13] a) X. Song, Y. Ge, H. Xu, S. Bao, L. Wang, X. Xue, Q. Yu, Y. Xing, Z. Wu, K. Xie, T. Zhu, P. Zhang, Y. Liu, Z. Wang, Z. Tie, J. Ma, Z. Jin, *J. Am. Chem. Soc.* **2024**, *146*, 7018–7028; b) W. Li, W. Liu, B. Huang, Z. Cai, H. Zhong, F. Guo, Y. Mai, *J. Mater. Chem. A* **2022**, *10*, 15449–15459; c) M. Fang, X. Yue, Y. Dong, Y. Chen, Z. Liang, *Joule* **2024**, *8*, 91–103.

[14] D. Zhang, Y. Liu, Z. Sun, Z. Liu, X. Xu, L. Xi, S. Ji, M. Zhu, J. Liu, *Angew. Chem. Int. Ed.* **2023**, *62*, e202310006.

[15] a) P. Zou, C. Wang, Y. He, H. L. Xin, *Angew. Chem. Int. Ed.* **2024**, *63*, e202319427; b) R. Xu, J. Yao, Z. Zhang, L. Li, Z. Wang, D. Song, X. Yan, C. Yu, L. Zhang, *Adv. Sci.* **2022**, *9*, e2204633; c) J. Han, M. J. Lee, J. H. Min, K. H. Kim, K. Lee, S. H. Kwon, J. Park, K. Ryu, H. Seong, H. Kang, E. Lee, S. W. Lee, B. J. Kim, *Adv. Funct. Mater.* **2024**, 2310801.

[16] J. Chen, Z. Yang, X. Xu, Y. Qiao, Z. Zhou, Z. Hao, X. Chen, Y. Liu, X. Wu, X. Zhou, L. Li, S. L. Chou, *Adv. Mater.* **2024**.

[17] J. Zhang, H. Wu, X. Du, H. Zhang, L. Huang, F. Sun, T. Liu, S. Tian, L. Zhou, S. Hu, Z. Yuan, B. Zhang, J. Zhang, G. Cui, *Adv. Energy Mater.* **2022**, *13*, 2202529.

[18] Y. Ding, B. He, D. Wang, M. Avdeev, Y. Li, S. Shi, *Energy Mater. Adv.* **2023**, *4*, 0041.

[19] M. J. Lee, J. Han, K. Lee, Y. J. Lee, B. G. Kim, K. N. Jung, B. J. Kim, S. W. Lee, *Nature* **2022**, *601*, 217–222.

[20] H. Wang, J. Song, K. Zhang, Q. Fang, Y. Zuo, T. Yang, Y. Yang, C. Gao, X. Wang, Q. Pang, D. Xia, *Energy Environ. Sci.* **2022**, *15*, 5149–5158.

[21] a) Z. Zhao, X. Zhou, B. Zhang, F. Huang, Y. Wang, Z. Ma, J. Liu, *Angew. Chem. Int. Ed.* **2023**, *62*, e202308738; b) A. Wang, Y. Nie, Y. Zhao, D. Xu, L. Zhang, Z. Zhao, L. Ren, S. Zhou, X. Liu, J. Luo, *Adv. Funct. Mater.* **2024**; c) W. Liang, X. Zhou, B. Zhang, Z. Zhao, X. Song, K. Chen, L. Wang, Z. Ma, J. Liu, *Angew. Chem. Int. Ed.* **2024**, *63*.
[22] a) P. Jaumaux, Q. Liu, D. Zhou, X. Xu, T. Wang, Y. Wang, F. Kang, B. Li, G. Wang, *Angew. Chem. Int. Ed.* **2020**, *59*, 9134–9142; b) L. Wang, Y. He, H. L. Xin, *J. Electrochem. Soc.* **2023**, *170*, 090525.

Manuscript received: June 14, 2024
Accepted manuscript online: July 26, 2024
Version of record online: September 13, 2024